Supplementary Information

Supplementary Table 1. Primers sequences for mouse *Oct1*, *Oct2*, *Oct3*, *Mdr1a*, and *Gapdh*.

Genes		Primer sequence	References
mOct1	Forward	5′-GTAAGCTCTGCCTCCTGGTG-3′	1
	Reverse	5′-GCTGTCGTTCTCCTGTAGCC-3′	
mOct2	Forward	5′-TACCGGAGTCTCCAAGATGG-3′	1
	Reverse	5′-GACCAAGTCCAGGAACGAAG-3′	
mOct3	Forward	5'-CAGATATGGCAGGCTCATCA-3'	1
	Reverse	5'-GACTTGCTTCGTGATGCTGA-3'	
mMdr1a	Forward	5'-GATCAACTCGCAAAAGCATCTG-3'	2
	Reverse	5'-CCACTCCAGCTATCGCAATG-3'	
mGapdh	Forward	5′-TGTGTCCGTCGTGGATCTGA-3′	3
	Reverse	5′-CACCACCTTCTTGATGTCATCATAC-3′	

1. Lips KS, Wunsch J, Zarghooni S, Bschleipfer T, Schukowski K, Weidner W *et al.* Acetylcholine and molecular components of its synthesis and release machinery in the urothelium. *Eur Urol* 2007; **51**:1042-1153.
2. NM_011076.2
3. Shioda N, Beppu H, Fukuda T, Li E, Kitajima I, Fukunaga K. Aberrant calcium/calmodulin-dependent protein kinase II (CaMKII) activity is associated with abnormal dendritic spine morphology in the ATRX mutant mouse brain. *J Neurosci* 2011; **31**:346-358

Supplementary Table 2. N-methyl-R-SAL or 1-benzyl-TIQ inhibit MPP^+ uptake by MDCK-hOCT1 and MDCK-hOCT2 cells.

	K_M	V_{max}	K	K_i[b]
	μM	pmol/mg/min	μL/mg/min	μM
hOCT1				
MPP^+ only	7.3±1.9	1021.0±112.0	3.9±0.2	
+ N-methyl-R-SAL (0.1 mM)	44.7±8.7	1131.3±195.5	4.3±0.7	45.9
+ 1-benzyl-TIQ (0.05 mM)	21.7±3.7	1053.8±115.6	5.7±0.6	40.7
hOCT2				
MPP^+ only	5.1±1.0	296.1±34.6	2.5±0.3	
+ N-methyl-R-SAL (0.1 mM)	9.8±1.0[a]	302.6±14.7	3.9±1.8	186.0
+ 1-benzyl-TIQ (0.1 mM)	42.5±7.5[a]	326.4±6.8	1.8±0.4	18.0

Data are shown as the mean±SEM for three different preparations, each in triplicate.

[a] $p<0.05$ compared to MPP^+ only.

[b] the K_i values were estimated from the intercept on the x axis in the plot of inhibitor concentration vs. slope of the Lineweaver-Burk plot

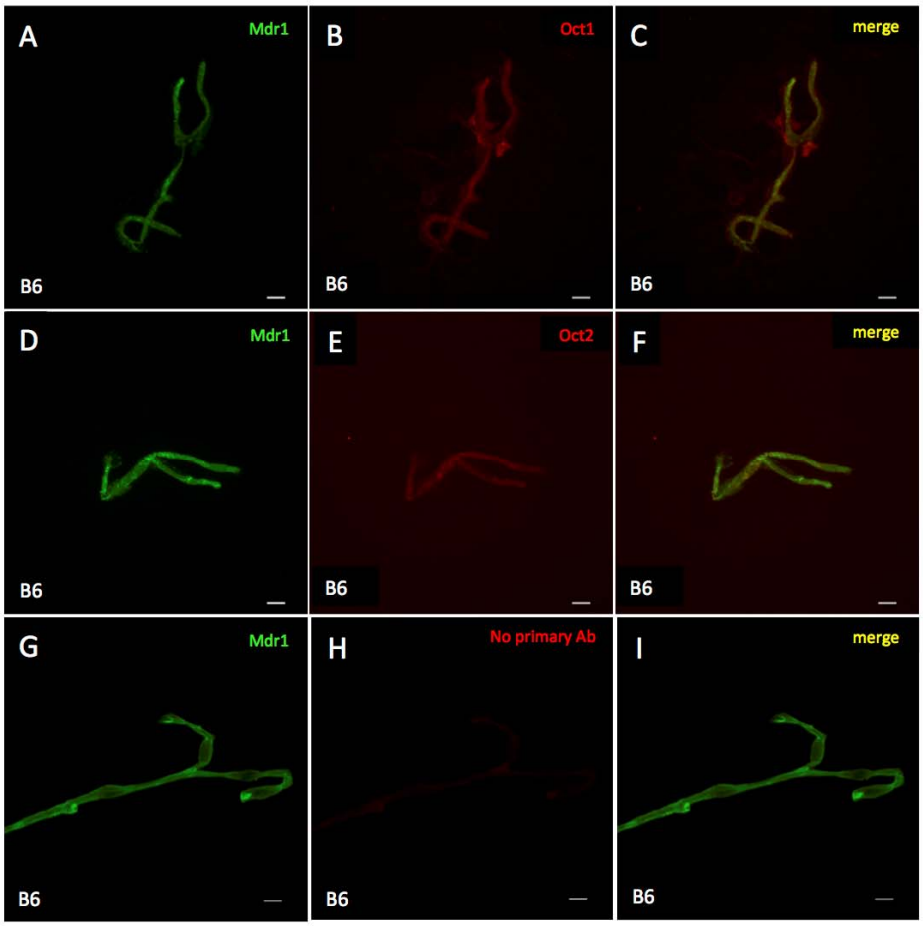

Supplementary Figure 1. Immunofluorescence staining of Mdr1 (green), Oct1 (red), and Oct2 (red) in brain microvessels isolated from B6 mice. (A-C) Protein expression of Mdr1(A), Oct1 (B) and co-localization of Mdr1 and Oct1 (C). (D-F) Protein expression of Mdr1 (D), Oct2 (E) and co-localization of Mdr1 and Oct2 (F). (G-I) Controls with primary anti-Octs antibodies omitted are also shown. Brain microvessels stained with Mdr1 (G) and secondary (anti-rabbit) antibodies without (H) or with (I) co-staining of Mdr1. Scale bars = 10 μm.

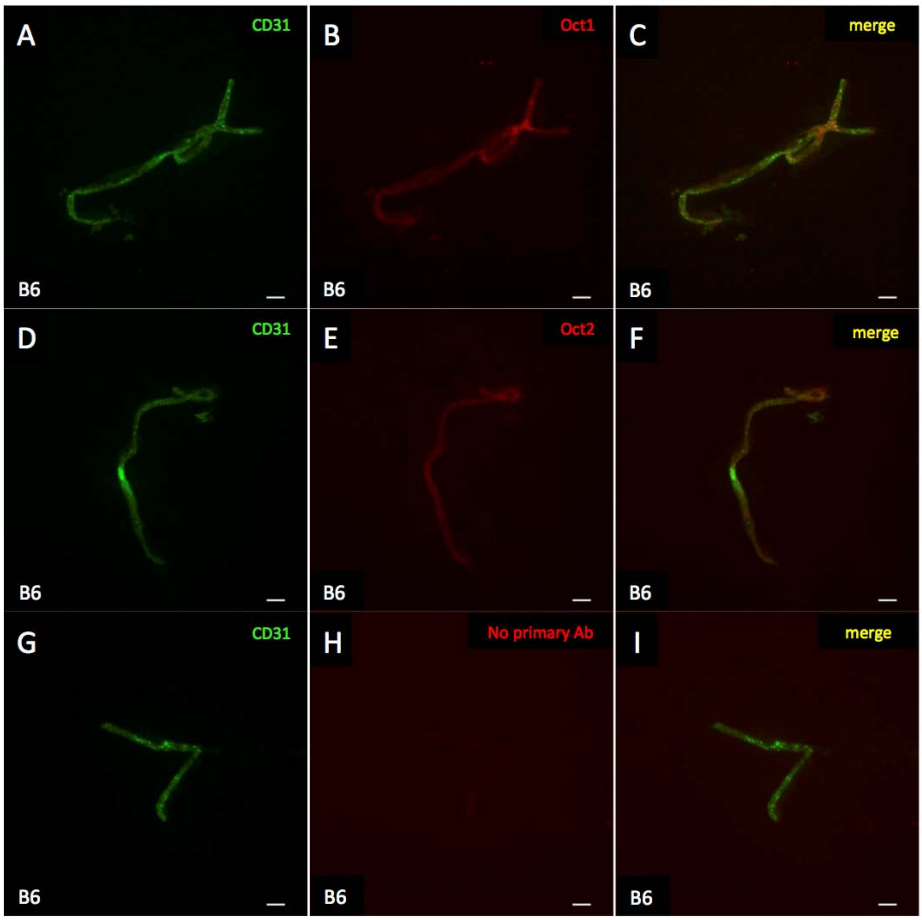

Supplementary Figure 2. Immunofluorescence staining of CD31 (green), Oct1 (red), and Oct2 (red) in brain microvessels isolated from B6 mice. (A-C) Protein expression of CD31 (A), Oct1 (B) and co-localization of CD31 and Oct1 (C). (D-F) Protein expression of CD31 (D), Oct2 (E) and co-localization of CD31 and Oct2 (F). (G-I) Controls with primary anti-Octs antibodies omitted are also shown. Brain microvessels stained with CD31 (G) and secondary (anti-rabbit) antibodies without (H) or with (I) co-staining of CD31. Scale bars = 10 μm.

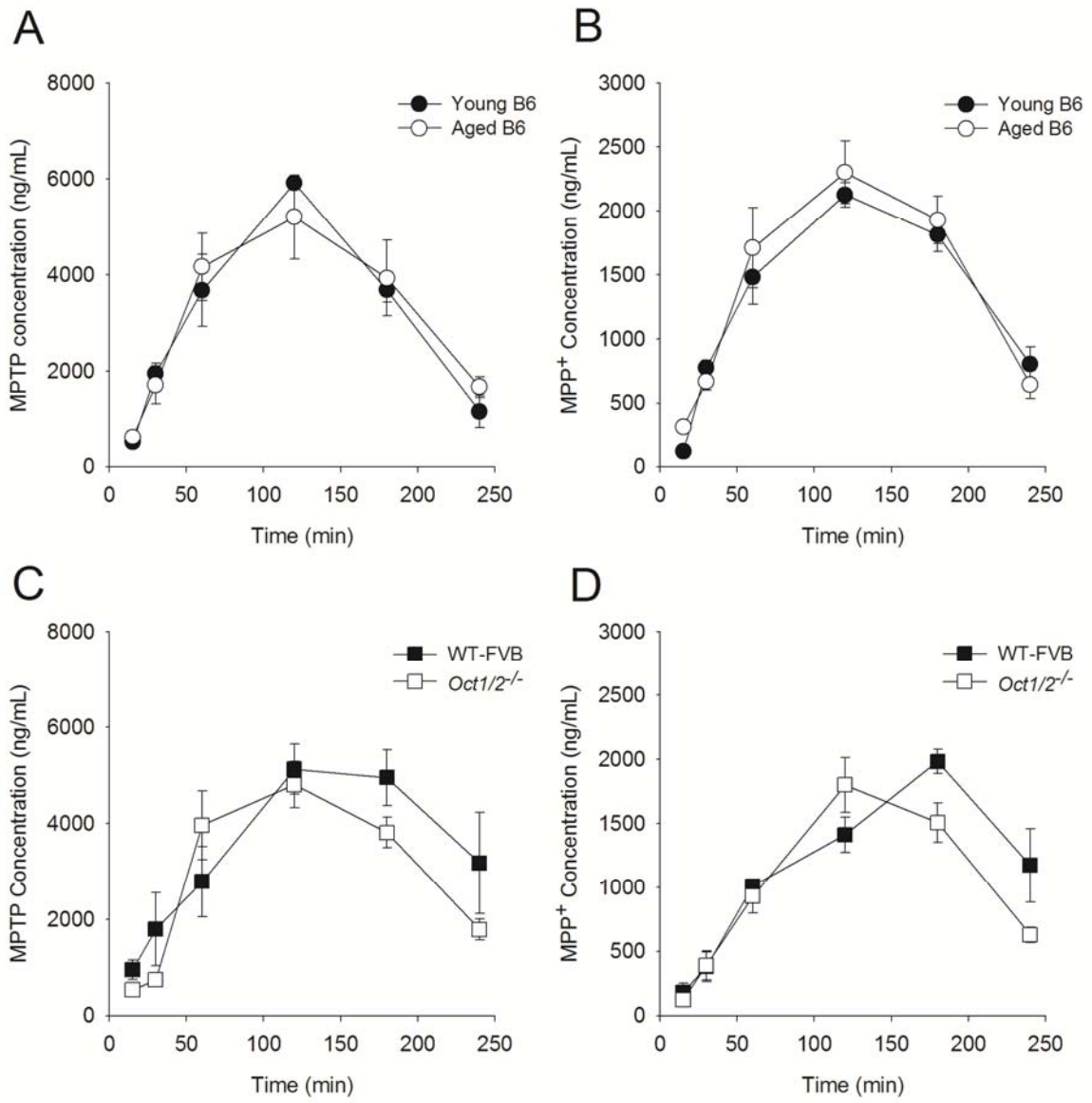

Supplementary Figure 3. Plasma concentrations of MPTP and MPP^+ in B6 mice, wild-type-FVB mice, and $Oct1/2^{-/-}$ mice after an intraperitoneal administration of 15 mg/kg MPTP. The results are shown for B6 mice at different ages (black and white circles for mice at 2 months and 15 months of age, respectively) (A and B), and for wild-type FVB mice (black squares) and $Oct1/2^{-/-}$ mice (white squares) at 2 months of age (C and D). The data are presented as the mean±SEM.

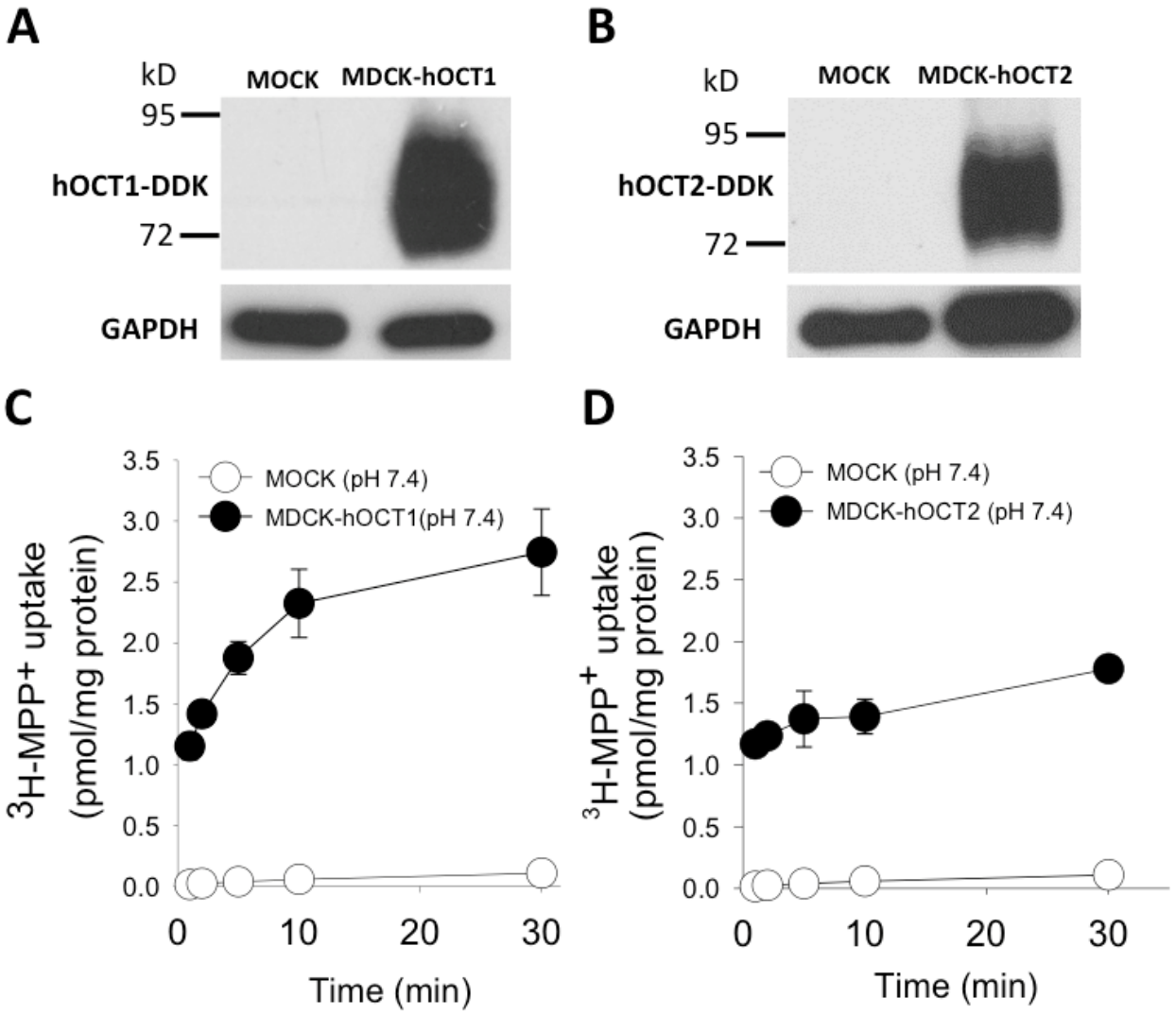

Supplementary Figure 4. (A and B) Western blots of hOCT1 and hOCT2 against the DDK-tag in the membrane fractions of MDCK-hOCT1 and MDCK-hOCT2 cells. (C and D) Time-dependent MPP^+ uptake by vector-transfected cells (MOCK), MDCK-hOCT1 cells (C), and MDCK-hOCT2 cells (D) at pH 7.4. The data are presented as the mean±SEM for 3 experiments, each in triplicate.